

NonLocal Means-based Speckle Filtering for Ultrasound Images

Pierrick Coupé^{1,2,4}, Pierre Hellier^{1,2,4}, Charles Kervrann^{3,5} and Christian Barillot^{1,2,4}

¹ University of Rennes I- CNRS UMR 6074, IRISA, Campus de Beaulieu, F-35042 Rennes, France

² INRIA, VisAGeS U746 Unit/Project, IRISA, Campus de Beaulieu, F-35042 Rennes, France

³ INRIA, VISTA Project, IRISA, Campus de Beaulieu, F-35042 Rennes, France

⁴ INSERM, VisAGeS U746 Unit/Project, IRISA, Campus de Beaulieu, F-35042 Rennes, France

⁵ INRA, UR341 Mathématiques et Informatique Appliquées, Domaine de Vilvert 78352 Jouy en Josas, France

Abstract

In image processing, restoration is expected to improve the qualitative inspection of the image and the performance of quantitative image analysis techniques. In this paper, an adaptation of the Non Local (NL-) means filter is proposed for speckle reduction in ultrasound (US) images. Originally developed for additive white Gaussian noise, we propose to use a Bayesian framework to derive a *NL-means* filter adapted to a relevant ultrasound noise model. Quantitative results on synthetic data show the performances of the proposed method compared to well-established and state-of-the-art methods. Results on real images demonstrate that the proposed method is able to preserve accurately edges and structural details of the image.

I. INTRODUCTION

In ultrasound imaging, denoising is challenging since the speckle artifacts cannot be easily modeled and are known to be tissue-dependent. In the imaging process, the energy of the high frequency waves are partially reflected and transmitted at the boundaries between tissues having different acoustic impedances. The images are also log-compressed to make easier visual inspection of anatomy with real-time imaging capability. Nevertheless, the diagnosis quality is often low and reducing speckle while preserving anatomic information is necessary to delineate reliably and accurately the regions of interest. Clearly, the signal-dependent nature of the speckle must be taken into account to design an efficient speckle reduction filter. Recently, it has been demonstrated that image patches are relevant features for denoising images in adverse situations [1]–[3]. The related methodology can be adapted to derive a robust filter for US images. Accordingly, in this paper we introduce a novel restoration scheme for ultrasound (US) images, strongly inspired from the NonLocal (NL-) means approach [1] introduced by Buades *et al.* [1] to denoise 2D natural images corrupted by an additive white Gaussian noise. In this paper, we propose an adaptation of the NL-means method to a dedicated US noise model [4] using a Bayesian motivation for the NL-means filter [3]. In what follows, invoking the central limit theorem, we will assume that the observed signal at a pixel is a Gaussian random variable with mean zero and a variance determined by the scattering properties of the tissue at the current pixel.

The remainder of the paper is organized as follows. In Section II, we give an overview of speckle filters and related methods. Section III described the proposed Bayesian NL-means filter adapted to speckle noise. Quantitative results on artificial images with various noise models are presented in Section IV. Finally, qualitative result on real 2D and 3D US images are proposed in Section V.

II. SPECKLE REDUCTION: RELATED WORK

The speckle in US images is often considered as undesirable and several noise removal filters have been proposed. Unlike the additive white Gaussian noise model adopted in most denoising methods, US imaging requires specific filters due to the signal-dependent nature of the speckle intensity. In this section, we present a classification of standard adaptive filters and methods for speckle reduction.

A. Adaptive Filters

The adaptive filters are widely used in US image restoration because they are easy to implement and control. The commonly-used adaptive filters - the Lee's filter [5], Frost's filter [6], and Kuan's filter [7] - assume that speckle noise is essentially a multiplicative noise. Many improvements of these classical filters have been proposed since. At the beginning of the 90's, Lopes *et al.* [8] suggested to improve the Lee's and Frost's filters by classifying the pixels in order to apply specific processing to the different classes. Based on this idea, the so-called Adaptive Speckle Reduction filter (ASR) exploits local image statistics to determine specific areas to be processed further. In [9], the kernel of the adaptive filter is fitted to homogeneous regions according to local image statistics. Analyzing local homogeneous regions was also investigated in [10], [11] to spatially adapt the filter parameters. Note that the Median filter has been also examined for speckle reduction in [4]. Very recently, a stochastic approach to ultrasound despeckling (SBF) has been developed in [12], [13]. This local averaging method removes the local extrema assumed to be outliers in a robust statistical estimation framework. Finally, the Rayleigh-Maximum-Likelihood (R-ML) filter has been derived with similar methodological tools in [14].

B. Partial Differential Equations (PDE) -based approaches

Adapted formulations of the Anisotropic Diffusion filter (AD) [15] and the Total Variation minimization scheme (TV) [16] have been developed for US imaging. In [17], [18], the Speckle Reducing Anisotropic Diffusion (SRAD) was introduced and involves a noise-dependent instantaneous coefficient of variation. In [19] the Nonlinear Coherent Diffusion (NCD) filter is based on the assumption that the multiplicative speckle in US signals is transformed into an additive Gaussian noise in Log-compressed images. Recently, the Oriented SRAD (OSRAD) filter has been proposed in [20]; this filter takes into account the local directional variance of the image intensity, i.e., the local image geometry. Finally, the TV minimization scheme has been adapted to ultrasound imaging in [21], [22]. Unlike the previous adaptive speckle filters, all the considered PDE-based approaches are iterative and produce smooth images while preserving edges. Nevertheless, meaningful structural details are unfortunately removed during iterations.

C. Multiscale methods

Several conventional wavelet thresholding methods [23]–[25] have also been investigated for speckle reduction [26]–[28] with the assumption that the logarithm compression of US images transforms the speckle into an additive Gaussian noise. In order to relax this restrictive assumption, Pizurica *et al.* [29] proposed a wavelet-based Generalized Likelihood ratio formulation and imposed no prior on noise and signal statistics. In [30]–[33], the Bayesian framework was also explored to perform wavelet thresholding adapted to the non-Gaussian statistics of the signal. Note that other multiscale strategies have been also studied in [34]–[36] to improve the performance of the AD filter; in [37], the Kuan's filter is applied to interscale layers of a Laplacian pyramid.

D. Hybrid approaches

The aforementioned approaches can be also combined in order to take advantage of the different paradigms. In [38], the image is preprocessed by an adaptive filter in order to decompose the image into two components. A Donoho's soft thresholding method is then performed on each component. Finally, the two processed components are combined to reduce speckle. PDE-based approaches and a wavelet transform have been also combined as proposed in [39].

III. METHOD

The previously mentioned approaches for speckle reduction are based on the so-called *locally adaptive recovery paradigm* [40]. Nevertheless, more recently, a new *patch-based non local recovery paradigm* has been proposed by Buades *et al* [1]. This new paradigm proposes to replace the local comparison of pixels by the non local comparison of patches. Unlike the aforementioned methods, the so-called *NL-means* filter does not make any assumptions about the location of the most relevant pixels used to denoise the current pixel. The weight assigned to a pixel in the restoration of the current pixel does not depend on the distance between them (neither in terms of spatial distance nor in terms of intensity distance). The local model of the signal is revised and the authors consider only information redundancy in the image. Instead of comparing the intensity of the pixels, which may be highly corrupted by noise, the *NL-means* filter analyzes the patterns around the pixels. Basically, image patches are compared for selecting the relevant features useful for noise reduction. This strategy leads to competitive results when compared to most of the state-of-the-art methods [3], [41]–[46]. Nevertheless, the main drawback of this filter is its computational burden. In order to overcome this problem, we have recently proposed a fast and optimized implementation of the *NL-means* filter for 3D Magnetic Resonance (MR) images [46].

In this section, we rather revise the traditional formulation of the *NL-means* filter, suited to the additive white Gaussian noise model, and adapt this filter to spatial speckle patterns. Accordingly, a dedicated noise model used for US images is first considered. A Bayesian formulation of the *NL-means* filter [3] is then used to derive a new speckle filter.

A. The Non Local means Filter

Let us consider a gray-scale noisy image $u = (u(x_i))_{x_i \in \Omega^{dim}}$ defined over a bounded domain $\Omega^{dim} \subset \mathbb{R}^{dim}$, (which is usually a rectangle of size $|\Omega^{dim}|$) and $u(x_i) \in \mathbb{R}_+$ is the noisy observed intensity at pixel $x_i \in \Omega^{dim}$. In the following, dim denotes the image grid dimension ($dim = 2$ or $dim = 3$ respectively for 2D and 3D images). We also use the notations given below:

Original pixelwise *NL-means* approach

- Δ_i : square search volume centered at pixel x_i of size $|\Delta_i| = (2M + 1)^{dim}$, $M \in \mathbb{N}$;
- \mathcal{N}_i : square local neighborhood of x_i of size $|\mathcal{N}_i| = (2d + 1)^{dim}$, $d \in \mathbb{N}$;
- $\mathbf{u}(\mathcal{N}_i)$: vector $(u^{(1)}(\mathcal{N}_i), \dots, u^{(|\mathcal{N}_i|)}(\mathcal{N}_i))^T$ gathering the intensity values of \mathcal{N}_i ;
- $v(x_i)$: true intensity value at pixel $x_i \in \Omega^{dim}$;
- $NL(u)(x_i)$: restored value of pixel x_i ;
- $w(x_i, x_j)$: weight used for restoring $u(x_i)$ given $u(x_j)$ and based on the similarity of patches $\mathbf{u}(\mathcal{N}_i)$ and $\mathbf{u}(\mathcal{N}_j)$.

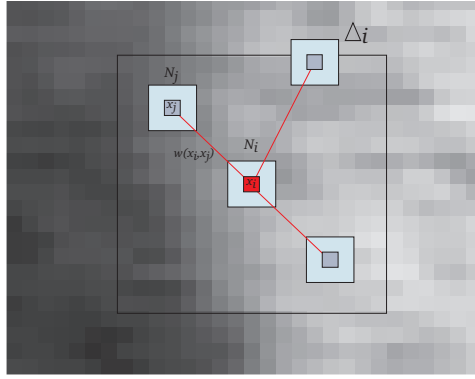


Fig. 1. **Pixelwise NL-means filter** ($d = 1$ and $M = 8$). The restored value at pixel x_i (in red) is the weighted average of all intensity values of pixels x_j in the search volume Δ_i . The weights are based on the similarity of the intensity neighborhoods (patches) $\mathbf{u}(\mathcal{N}_i)$ and $\mathbf{u}(\mathcal{N}_j)$.

Blockwise NL-means approach

B_i : square block centered at x_i of size $|B_i| = (2\alpha + 1)^{dim}$, $\alpha \in \mathbb{N}$;

- $\mathbf{v}(B_i)$: unobserved vector of true values of block B_i ;

$\mathbf{u}(B_i)$: vector gathering the intensity values of block B_i ;

$\mathbf{NL}(u)(B_i)$: restored block of pixel x_i ;

$w(B_i, B_j)$: weight used for restoring $\mathbf{u}(B_i)$ given $\mathbf{u}(B_j)$ and based on the similarity of blocks $\mathbf{u}(B_i)$ and $\mathbf{u}(B_j)$.

Finally, the blocks B_{i_k} are centered on pixels x_{i_k} with $i_k = (k_1 n, \dots, k_{dim} n)$, $(k_1, \dots, k_{dim}) \in \mathbb{N}^{dim}$ and n represents the distance between block centers.

1) *Pixelwise approach*: In the original NL-means filter [1], the restored intensity $NL(u)(x_i)$ of pixel x_i , is the weighted average of all the pixel intensities $u(x_i)$ in the image Ω^{dim} :

$$NL(u)(x_i) = \sum_{x_j \in \Omega^{dim}} w(x_i, x_j) u(x_j) \quad (1)$$

where $w(x_i, x_j)$ is the weight assigned to value $u(x_j)$ for restoring the pixel x_i . More precisely, the weight evaluates the similarity between the intensities of the local neighborhoods (patches) \mathcal{N}_i and \mathcal{N}_j centered on pixels x_i and x_j , such that $w(x_i, x_j) \in [0, 1]$ and $\sum_{x_j \in \Omega^{dim}} w(x_i, x_j) = 1$ (see Fig. 1). The size of the local neighborhood \mathcal{N}_i and \mathcal{N}_j is $(2d + 1)^{dim}$. The traditional definition of the NL-means filter considers that the intensity of each pixel can be linked to pixel intensities of the whole image. For practical and computational reasons, the number of pixels taken into account in the weighted average is restricted to a neighborhood, that is a “search volume” Δ_i of size $(2M+1)^{dim}$, centered at the current pixel x_i .

For each pixel x_j in Δ_i , the Gaussian-weighted Euclidean distance $\|\cdot\|_{2,a}^2$ is computed between the two image patches $\mathbf{u}(\mathcal{N}_j)$ and $\mathbf{u}(\mathcal{N}_i)$ as explained in [1]. This distance is the traditional L_2 -norm convolved with a Gaussian kernel of standard deviation a . The standard deviation of the Gaussian kernel is used to assign spatial weights to the patch elements. The central pixels in the patch contribute more to the distance than the pixels located at the periphery. The weights $w(x_i, x_j)$ are then computed as follows:

$$w(x_i, x_j) = \frac{1}{Z_i} \exp - \frac{\|\mathbf{u}(\mathcal{N}_i) - \mathbf{u}(\mathcal{N}_j)\|_{2,a}^2}{h^2} \quad (2)$$

where Z_i is a normalization constant ensuring that $\sum_{x_j \in \Omega^{dim}} w(x_i, x_j) = 1$, and h acts as a filtering parameter controlling the decay of the exponential function.

2) *Blockwise approach*: As presented in [46], a blockwise implementation of the proposed NL-means-based speckle filter is able to decrease the computational burden. The blockwise approach consists of: i) dividing the volume into blocks with overlapping supports; ii) performing a NL-means-like restoration of these blocks; iii) restoring the pixel intensities from the restored blocks. Here, we describe briefly these three steps and refer the reader to [46] for additional detailed explanations:

- a partition of the volume Ω^{dim} into overlapping blocks B_{i_k} containing $P = (2\alpha + 1)^{dim}$ elements is performed, i.e. $\Omega^{dim} = \bigcup_k B_{i_k}$. These blocks are centered on pixels x_{i_k} which constitute a subset of Ω^{dim} . The pixels x_{i_k} are equally distributed at positions $i_k = (k_1 n, k_2 n, k_3 n)$, $(k_1, k_2, k_3) \in \mathbb{N}^{dim}$ where n represents the distance between the centers of B_{i_k} ;

- a block B_{i_k} is restored as follows:

$$\mathbf{NL}(u)(B_{i_k}) = \sum_{B_j \in \Delta_{i_k}} w(B_{i_k}, B_j) \mathbf{u}(B_j) \quad \text{with} \quad w(B_{i_k}, B_j) = \frac{1}{Z_{i_k}} \exp - \frac{\|\mathbf{u}(B_{i_k}) - \mathbf{u}(B_j)\|_2^2}{h^2} \quad (3)$$

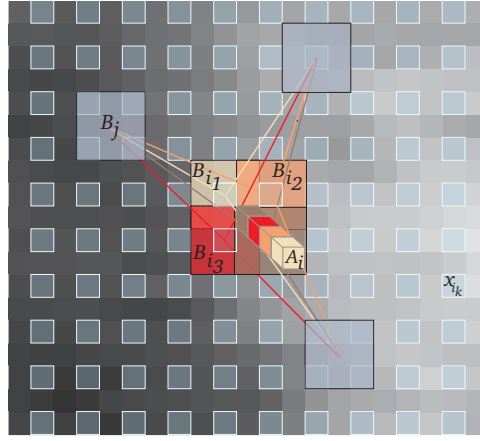


Fig. 2. **Blockwise NL-means Filter** ($n = 2$, $\alpha = 1$ and $L = 4$). For each block B_{i_k} centered at pixel x_{i_k} , a *NL-means*-like restoration is performed from blocks B_j . The restored value of the block B_{i_k} is the weighted average of all the blocks B_j in the search volume. For a pixel x_i included in several blocks, several estimates are obtained and fused. The restored value of pixel x_i is the average of the different estimations stored in vector \mathbf{A}_i .

where $\mathbf{u}(B_i) = (u^{(1)}(B_i), \dots, u^{(P)}(B_i))^T$ is an image patch gathering the intensities of the block B_i , Z_{i_k} is a normalization constant ensuring $\sum_{B_j \in \Delta_{i_k}} w(B_{i_k}, B_j) = 1$ and

$$\|\mathbf{u}(B_{i_k}) - \mathbf{u}(B_j)\|_2^2 = \sum_{p=1}^P (u^{(p)}(B_i) - u^{(p)}(B_j))^2; \quad (4)$$

iii) for a pixel x_i included in several blocks B_{i_k} , several estimates of the same pixel x_i from different $\mathbf{NL}(u)(B_{i_k})$ are computed and stored in a vector \mathbf{A}_i of size L (see Fig 2). We denote $\mathbf{A}_i(l)$ the l th element of vector \mathbf{A}_i . The final restored intensity of pixel x_i is the mean of the restored values $\mathbf{NL}(u)(B_{i_k})$.

The main advantage of this approach is to significantly reduce the complexity of the algorithm. Indeed, for a volume Ω^{dim} of size $|\Omega^{dim}|$, the global complexity is $\mathcal{O}((2\alpha + 1)^{dim} (2M + 1)^{dim} (\frac{N}{n})^{dim})$. For instance, if we set $n = 2$, the complexity is divided by a factor of 4 in 2D and 8 in 3D.

B. The NL Means-based Speckle Filter

1) *Bayesian formulation*: In [3], a Bayesian formulation of the *NL-means* filter was proposed. Equivalent to the conditional mean estimator, it has been shown that an empirical estimator $\hat{\mathbf{v}}(B_{i_k})$ of a block B_{i_k} can be defined as (see the appendix):

$$\hat{\mathbf{v}}(B_{i_k}) = \frac{\frac{1}{|\Delta_{i_k}|} \sum_{j=1}^{|\Delta_{i_k}|} \mathbf{v}(B_j) p(\mathbf{u}(B_{i_k}) | \mathbf{v}(B_j))}{\frac{1}{|\Delta_{i_k}|} \sum_{j=1}^{|\Delta_{i_k}|} p(\mathbf{u}(B_{i_k}) | \mathbf{v}(B_j))} \quad (5)$$

where $p(\mathbf{u}(B_{i_k}) | \mathbf{v}(B_j))$ denotes the probability density function (pdf) of $\mathbf{u}(B_{i_k})$ given the noise free and unknown patches $\mathbf{v}(B_j)$. Since $\mathbf{v}(B_j)$ is unknown, an estimator is classically computed by substituting $\mathbf{u}(B_j)$ for $\mathbf{v}(B_j)$. Hence, we get

$$\hat{\mathbf{v}}(B_{i_k}) = \frac{\sum_{j=1}^{|\Delta_{i_k}|} \mathbf{u}(B_j) p(\mathbf{u}(B_{i_k}) | \mathbf{u}(B_j))}{\sum_{j=1}^{|\Delta_{i_k}|} p(\mathbf{u}(B_{i_k}) | \mathbf{u}(B_j))} \quad (6)$$

where $p(\mathbf{u}(B_{i_k}) | \mathbf{u}(B_j))$ denotes the pdf of $\mathbf{u}(B_{i_k})$ conditionally to $\mathbf{u}(B_j)$. In the case of an additive white Gaussian noise, the likelihood $p(\mathbf{u}(B_{i_k}) | \mathbf{u}(B_j))$ will be proportional to $e^{-\frac{\|\mathbf{u}(B_{i_k}) - \mathbf{u}(B_j)\|_2^2}{h^2}}$, and the corresponding Bayesian estimator $\hat{\mathbf{v}}(B_{i_k})$ is then similar to the initial *NL-means* method (see (3)).

In what follows, this general Bayesian formulation is used to derive an adapted filter to a dedicated ultrasound noise model.

2) *Noise models for log-compressed US images:* The relevant noise pdfs useful for US image denoising cannot be easily exhibited. Basically, we should consider the complex image formation process, i.e.: *i)* local correlation due to periodic arrangements of scatterers [17] and finite beamwidth; *ii)* envelope detection and logarithm amplification of radio-frequency signals performed on the display image [19]; *iii)* additive Gaussian noise of sensors [19]; *iv)* additive Gaussian noise introduced by the acquisition card. All these factors tend to prove that the Rayleigh model used for RF signals is not suitable for analyzing US Log-compressed images. Usually, in the wavelet denoising domain [19], [26], [27], multiplicative speckle noise is supposed to be transformed into an additive Gaussian noise by the logarithmic compression. However, recent studies related to US images demonstrate also that the distribution of noise is satisfyingly approximated by a Gamma distribution [47] or a Fisher-Tippett distribution [48].

Consequently, we have decided to choose the following general speckle model:

$$u(x) = v(x) + v^\gamma(x)\eta(x) \quad (7)$$

where $v(x)$ is the original image, $u(x)$ is the observed image, $\eta(x) \sim \mathcal{N}(0, \sigma^2)$ is a zero-mean Gaussian noise. This model is more flexible and less restrictive than the usual RF model and is able to capture reliably image statistics since the factor γ depends on ultrasound devices and additional processing related to image formation.

Contrary to additive white Gaussian noise model, the noise component in (7) is image-dependent. In [4], based on the experimental estimation of the mean versus the standard deviation in Log-compressed images, Loupas *et al.* have shown that $\gamma = 0.5$ model fits better to data than the multiplicative model or the Rayleigh model. Since, this model has been used successfully in many studies [38], [49]–[51]. Clearly, this model is relevant since it is confirmed that the speckle is higher in regions of high intensities versus regions of low intensities [47], [49].

3) *A new statistical distance for patch comparison: the Pearson distance:* Based on the Bayesian formulation (see (6)), we introduce a new distance to compare image patches if we consider the noise model (7). For each pixel we assume:

$$u(x)|v(x) \sim \mathcal{N}(v(x), v(x)^{2\gamma}\sigma^2) \quad (8)$$

which yields

$$p(u(x)|v(x)) \propto \exp - \frac{(u(x) - v(x))^2}{2v(x)^{2\gamma}\sigma^2}. \quad (9)$$

Given a block B_i , the likelihood can be factorized as (conditional independence hypothesis):

$$\begin{aligned} p(\mathbf{u}(B_i)|\mathbf{u}(B_j)) &= \prod_{p=1}^P p(u^{(p)}(x_i)|u^{(p)}(x_j)) \\ &\propto \exp - \sum_{p=1}^P \frac{(u^{(p)}(x_i) - u^{(p)}(x_j))^2}{2(u^{(p)})^{2\gamma}(x_j)\sigma^2}. \end{aligned} \quad (10)$$

Accordingly, the so-called Pearson distance defined as

$$d_P(\mathbf{u}(B_i), \mathbf{u}(B_j)) = \sum_{p=1}^P \frac{(u^{(p)}(B_i) - u^{(p)}(B_j))^2}{(u^{(p)})^{2\gamma}(B_j)} \quad (11)$$

is substituted to the usual L_2 -norm (see (4)). In the reminder of the paper, $\gamma = 0.5$ is considered in the proposed filter.

A pixel selection scheme similar to [46] based on tests on the mean will be used to select the most relevant patches. This selection is controlled by the thresholding μ_1 as previously described in [46]. As a result, the denoising results are improved and the algorithm is faster. In addition, a parallel implementation is used in all experiments to speed up the algorithm.

IV. SYNTHETIC IMAGES EXPERIMENTS

In this section, we propose to compare different filters with experiments on synthetic data, with different noise models, image data and quality criteria. Two simulated data are described in this section:

- in section IV-A, a 2D phantom and a noise model available in MATLAB are considered for the experiments, and the signal-to-noise Ratio (SNR) is used to compare objectively several methods;
- in section IV-B, the realistic speckle simulation proposed in Field II is performed and the ultrasound despeckling assessment index (\hat{Q}) proposed in [12], [13] is chosen for objective comparisons;

Filter	iteration number $\sigma = \{0.2; 0.4; 0.8\}$	smoothing parameter $\sigma = \{0.2; 0.4; 0.8\}$	threshold	patch size
Lee's filter	-	-	-	2×2
Kuan's filter	-	-	-	2×2
SBF	$\{5; 8; 30\}$	-	-	3×3
SRAD	$\{500; 1000; 2000\}$	$dt = \{0.1; 0.2; 0.1\}$	-	-
NL-means	-	$h = \{20.0; 25.0; 30.0\}$	-	5×5
OBNLM	-	$h = \{12.0; 14.0; 16.0\}$	$\mu_1 = 0.9$	5×5

TABLE I

OPTIMAL SET OF PARAMETERS USED FOR THE MATLAB "PHANTOM" EXPERIMENT. FOR THE *NL-means* BASED FILTERS, WE SET $n = 2$ AND

$$|\Delta_{i_k}| = 11 \times 11.$$

A. 2D phantom corrupted by the theoretical (MATLAB) noise model

1) *Speckle model and quality criterion*: In this experiment, the synthetic image "Phantom" (see Fig. 3), available in MATLAB, was corrupted with different levels of noise. The "Phantom" image is a 32 bit image of 256×256 pixels. First, an offset of 0.5 was added to the image (to avoid naught areas) before performing a multiplication of intensities by a factor 20. Then, the MATLAB speckle simulation based on the following image model

$$u(x_i) = v(x_i) + v(x_i)\nu(x_i), \quad \nu(x_i) \sim \mathcal{N}(0, \sigma^2) \quad (12)$$

was applied to the "Phantom" image. Three levels of noise were tested by setting $\sigma = \{0.2; 0.4; 0.8\}$. To assess denoising methods, the SNR values [52] were computed between the "ground truth" and the denoised images :

$$SNR = 10 \log_{10} \frac{\sum_{x_i \in \Omega^2} (v(x_i)^2 + \hat{v}(x_i)^2)}{\sum_{x_i \in \Omega^2} (v(x_i) - \hat{v}(x_i))^2} \quad (13)$$

where $v(x_i)$ is the true value of pixel x_i and $\hat{v}(x_i)$ the restored intensity of pixel x_i .

2) *Compared methods*: In this experiment, we compared several speckle filters and the parameters were adjusted to get the best SNR values:

- Lee's filter (2D MATLAB implementation) [5]
- Kuan's filter (2D MATLAB implementation) [7]
- SBF filter (2D MATLAB implementation provided by the authors) [12]
- Speckle Reducing Anisotropic Diffusion (SRAD) (MATLAB implementation of Virginia University¹) [17]
- blockwise implementation of the classical *NL-means* filter [1]
- blockwise implementation of the proposed method denoted as Optimized Bayesian *NL-means* with block selection (OBNLM).

In this experiment, we have chosen to compare our method with well-known adaptive filters, such as the Lee's and Kuan's filters, and with two competitive state-of-the-art methods: SRAD and SBF filters. We limited the comparison to this set of methods but the results produced by other recent filters could be also analyzed further (e.g. see [14]). Moreover, the usual NL-means filter has been applied to the same images in order to quantitatively evaluate the performance of our speckle-based NL-means filter. For each method and for each noise level, the optimal filter parameters were searched within large ranges. These parameters are given in Table I.

3) *Results*: Table II gives the SNR values obtained for each method. The denoised images corresponding to $\sigma = 0.4$ are presented in Fig. 3. For all levels of noise, the OBNLM filter obtained the best SNR value. For this experiment, the use of the Pearson distance combined with block selection enabled to improve the denoising performances of the *NL-means* filter for images corrupted by signal-dependent noise. Visually, the *NL-means* based filter satisfyingly removed the speckle while preserving meaningful edges.

B. Field II simulation

1) *Speckle model and quality assessment*: In order to evaluate the denoising filters with a more relevant and challenging simulation of speckle noise, the validation framework proposed in [12], [13] was used. This framework is based on Field II simulation [53]. The "Cyst" phantom is composed of 3 constant classes C_r presented in Fig. 4. The result of the Field II simulation is converted into an 8 bit image of size 390×500 pixels. Since the geometry of the image is known, but not the true value of the image (i.e. without speckle), the authors introduced the ultrasound despeckling assessment index (\tilde{Q}) defined as:

¹<http://viva.ee.virginia.edu/downloads.html>

SNR (dB)			
Filter	$\sigma = 0.2$	$\sigma = 0.4$	$\sigma = 0.8$
Noisy phantom	39.32	25.96	14.11
Lee's filter	49.41	42.71	32.31
Kuan's filter	49.43	42.71	32.33
SBF	49.61	43.86	38.04
SRAD	57.17	44.07	33.29
NL-means	62.15	47.92	38.72
OBNLM	<u>64.13</u>	<u>53.12</u>	<u>42.13</u>

TABLE II

SNR VALUES OBTAINED WITH SEVERAL FILTERS APPLIED TO THE 2D MATLAB "PHANTOM" IMAGE.

Filter	iteration number	smoothing parameter	threshold	patch size
SBF	400	-	-	5×5
SRAD	500	$dt = 0.05$	-	-
NL-means	-	$h = 50$	-	11×11
OBNLM	-	$h = 50$	$\mu_1 = 0.75$	11×11

TABLE III

OPTIMAL SET OF PARAMETERS USED FOR VALIDATION ON THE 2D SYNTHETIC DATA SIMULATED WITH FIELD II. FOR THE *NL-means*-BASED FILTERS $n = 4$ AND $|\Delta_{i_k}| = 33 \times 33$.

$$Q = \frac{\sum_{r \neq l} (\mu_{C_r} - \mu_{C_l})^2}{\sum_r \sigma_{C_r}^2} \quad (14)$$

to evaluate the performance of denoising filters for this simulation. We denote μ_{C_r} as the mean and $\sigma_{C_r}^2$ as the variance of class C_r after denoising. To avoid the sensitivity to image resolution, Q is normalized by Q_{id} . The new index $\tilde{Q} = Q/Q_{id}$ is high if the applied filter is able to produce a new image with well separated classes and small variances for each class. According to [12], [13], an image is satisfyingly denoised if \tilde{Q} is high enough.

2) *Method Comparison*: For this experiment, we compared the SBF filter, SRAD filter, *NL-means* filter and the proposed OBNLM filter. The filter parameters are given in Table III. Compared to the previous experiment, the patch size by using the *NL-means*-based filters is increased. Indeed, the patch size reflects the scale of the "noise" compared to the image resolution. In the previous experiment, the resolution of the added noise was about one pixel. In this experiment, the objects to be removed are composed of several pixels, thus the patch size is increased to evaluate the restoration performance of each object.

3) *Results*: The denoised images and the quantitative results are given in Fig. 4. In this evaluation framework, the OBNLM filter produced the highest \tilde{Q} index. Similar values than those presented in [12], [13] were found for the SRAD and SBF filters. Compared to the original *NL-means* filter, the proposed adaptations for US images improved the \tilde{Q} index of the denoised image.

V. EXPERIMENTS ON REAL DATA

In this section, a visual comparison of 2D intraoperative ultrasound brain images (Section V-A) and a visual inspection of 3D ultrasound image of a liver (Section V-B) are proposed.

A. Intraoperative ultrasound brain images

In this paragraph, we propose a visual comparison of the SBF and SRAD filters and the OBNLM method on real intraoperative brain images. The parameters for the SBF and SRAD filters are the parameters given respectively in [17] and [12]. The parameters of the OBNLM filter were set as follows : $h = 8$, $n = 2$, $\alpha = 3$, $M = 6$ and $\mu_1 = 0.6$.

Figure 5 shows the denoising results. Visually, the OBNLM filter efficiently removes the speckle component while enhancing the edges and preserving the image structures. The visual results produced on real image by our method are competitive compared to SRAD and SBF filters.

B. Experiments on a 3D liver image

In this section, result of the proposed filter on 3D US image is proposed. These data are freely available on Cambridge University website². The B-scans were acquired with a Lynx ultrasound unit (BK Medical System) and tracked by the magnetic tracking system miniBIRD (Ascension Technology). The reconstruction of the volume was performed with the method described in [54]. The reconstructed volume size was $308 \times 278 \times 218$ voxels with an isotropic resolution of $0.5 \times 0.5 \times 0.5$ mm³.

The denoising results obtained with the OBNLM method on the liver volume are shown in Fig. 6. As for the previous experiment on 2D US brain images, the visual results on this 3D dataset show edge preservation and efficient noise removal produced by our filter.

²<http://mi.eng.cam.ac.uk/milab.html>

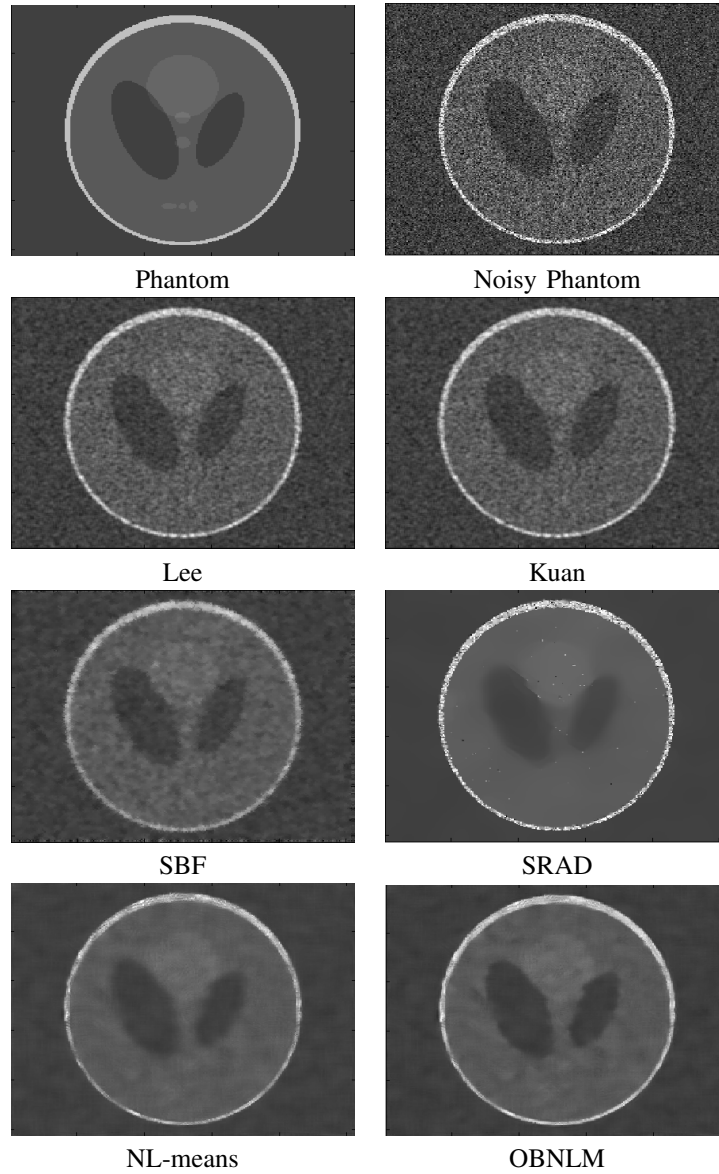


Fig. 3. Results obtained with different filters applied to the “Phantom” image corrupted with signal-dependent noise ($\sigma = 0.4$). The quantitative evaluation, measured using the signal-to-noise ratio, is presented in Table II.

Figure 7 shows zooming views of hepatic vessels. The edge preservation of the OBNLM filter is visible on the removed noise image that does not contain structures. Moreover, the difference in dark areas (hepatic vessels) and gray areas (hepatic tissues) shows the smoothing adaptation according to the signal intensity. The noise in brighter areas is drastically reduced.

VI. CONCLUSION

In this paper, we proposed a Non Local (NL)-means-based filter for ultrasound images by introducing the Pearson distance as a relevant criterion for patch comparison. Experiments were carried out on synthetic images with different simulations of speckle. During the experiments, quantitative measures were used to compare several denoising filters. Experiments showed that the Optimized Bayesian Non Local Means (OBNLM) filter proposes competitive performances compared to other state-of-the-art methods. Moreover, as assessed by quantitative results, our adaptation of classical NL-means filter to speckle noise proposes a filter more suitable for US imaging. Experiments on real ultrasound data were conducted and showed that the OBNLM method is very efficient at smoothing homogeneous areas while preserving edges. Further work will be pursued on the automatic tuning of the OBNLM filter and on the influence study on post-processing tasks such as image registration or image segmentation.

ACKNOWLEDGMENT

The authors thank Peter Tay for providing the MATLAB code of the SBF filter. The authors thank the reviewers for their fruitful comments.

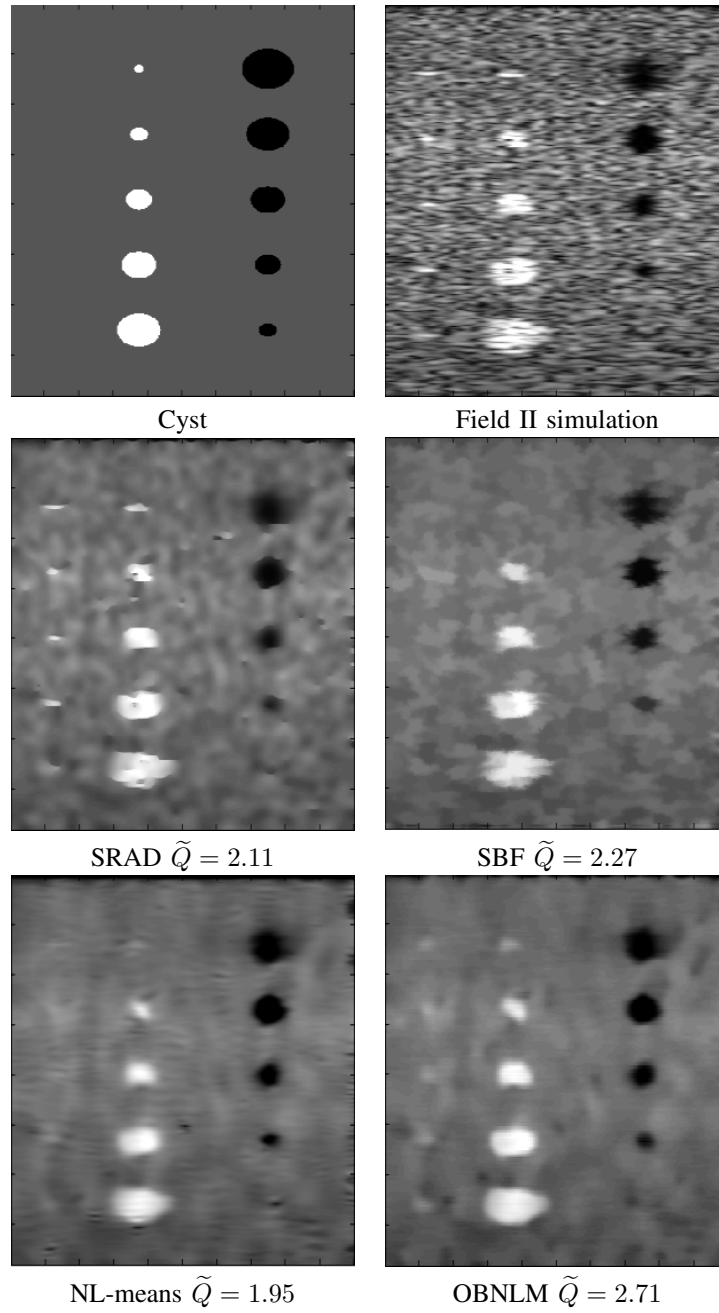


Fig. 4. Denoised images obtained with the compared filters for the Field II experiment and the corresponding \tilde{Q} indexes.

APPENDIX

Details of the Bayesian NL-means filter

The following Bayesian definition of the *NL-means* filter is presented in [3]. By considering the quadratic loss function, the optimal Bayesian estimator of a noise-free patch $\hat{\mathbf{v}}_{opt}(B)$ can be written as:

$$\hat{\mathbf{v}}_{opt}(B) = \underset{\mathbf{v}(B)}{\operatorname{argmin}} \sum_{\mathbf{v}(B)} \|\mathbf{v}(B) - \hat{\mathbf{v}}(B)\|^2 p(\mathbf{v}(B)|\mathbf{u}(B)) = \sum_{\mathbf{v}(B)} \mathbf{v}(B) p(\mathbf{v}(B)|\mathbf{u}(B)) \quad (15)$$

where $p(\mathbf{v}(B)|\mathbf{u}(B))$ denotes the probability density function (pdf) of $\mathbf{v}(B)$ conditionally to $\mathbf{u}(B)$, $\mathbf{u}(B)$ is the observed intensity and $\mathbf{v}(B)$ is the true intensity of block B . According to the Bayes' and marginalization rules, the *so-called* conditional mean estimator can be rewritten as (see [3]) :

$$\hat{\mathbf{v}}_{opt}(B) = \sum_{\mathbf{v}(B)} \mathbf{v}(B) \frac{p(\mathbf{v}(B)|\mathbf{u}(B))}{p(\mathbf{u}(B))} = \frac{\sum_{\mathbf{v}(B)} \mathbf{v}(B) p(\mathbf{u}(B)|\mathbf{v}(B)) p(\mathbf{v}(B))}{\sum_{\mathbf{v}(B)} p(\mathbf{u}(B)|\mathbf{v}(B)) p(\mathbf{v}(B))} \quad (16)$$

where $p(\mathbf{u}(B)|\mathbf{v}(B))$ denotes the distribution of $\mathbf{u}(B)$ conditionally to $\mathbf{v}(B)$. Since $p(\mathbf{u}(B)|\mathbf{v}(B))$ and $p(\mathbf{u}(v))$ cannot be estimated from only one realization of the image, these pdfs are estimated from observations (blocks B_j) taken in a search window Δ_i of a block B_i . According to [3], [55], the following approximations can be written:

$$\frac{1}{|\Delta_i|} \sum_{j=1}^{|\Delta_i|} \mathbf{v}(B_j) p(\mathbf{u}(B_i)|\mathbf{v}(B_j)) \xrightarrow{P} \sum_{\mathbf{v}(B)} \mathbf{v}(B) p(\mathbf{u}(B)|\mathbf{v}(B)) p(\mathbf{v}(B)) \quad (17)$$

$$\frac{1}{|\Delta_i|} \sum_{j=1}^{|\Delta_i|} p(\mathbf{u}(B_i)|\mathbf{v}(B_j)) \xrightarrow{P} \sum_{\mathbf{v}(B)} p(\mathbf{u}(B)|\mathbf{v}(B)) p(\mathbf{v}(B)), \quad (18)$$

If we assume the prior distribution $p(\mathbf{v}(B))$ uniform. This leads to the empirical Bayesian estimator $\hat{\mathbf{v}}(B_{i_k})$ uses in (5):

$$\hat{\mathbf{v}}(B_i) = \frac{\frac{1}{|\Delta_i|} \sum_{j=1}^{|\Delta_i|} \mathbf{v}(B_j) p(\mathbf{u}(B_i)|\mathbf{v}(B_j))}{\frac{1}{|\Delta_i|} \sum_{j=1}^{|\Delta_i|} p(\mathbf{u}(B_i)|\mathbf{v}(B_j))}. \quad (19)$$

We refer the reader to [3] for detailed explanations.

REFERENCES

- [1] A. Buades, B. Coll, and J. M. Morel, "A review of image denoising algorithms, with a new one," *Multiscale Modeling & Simulation*, vol. 4, no. 2, pp. 490–530, 2005.
- [2] S. P. Awate and R. T. Whitaker, "Unsupervised, information-theoretic, adaptive image filtering for image restoration," *IEEE Trans. Pattern Anal. Mach. Intell.*, vol. 28, no. 3, pp. 364–376, 2006.
- [3] C. Kervrann, J. Boulanger, and P. Coupé, "Bayesian non-local means filter, image redundancy and adaptive dictionaries for noise removal," in *Proc. Conf. Scale-Space and Variational Meth. (SSVM' 07)*, Ischia, Italy, June 2007, pp. 520–532.
- [4] T. Loupas, W. McDicken, and P. Allan, "An adaptive weighted median filter for speckle suppression in medical ultrasound image," *IEEE T. Circ. Syst.*, vol. 36, pp. 129–135, 1989.
- [5] J. S. Lee, "Digital image enhancement and noise filtering by use of local statistics," *IEEE Transactions on Pattern Analysis and Machine Intelligence*, vol. 2, pp. 165–168, 1980. [Online]. Available: http://adsabs.harvard.edu/cgi-bin/nph-bib_query?bibcode=1980ITPAM...2..165L
- [6] V. Frost, J. Stiles, K. Shanmugan, and J. Holtzman, "A model for radar images and its application to adaptive digital filtering of multiplicative noise," *IEEE Transactions on Pattern Analysis and Machine Intelligence*, vol. 2, pp. 157–65, 1982.
- [7] D. Kuan, A. Sawchuck, T. Strand, and P. Chavel, "Adaptive noise smoothing filter for images with signal-dependent noise," *IEEE Transactions on Pattern Analysis and Machine Intelligence*, vol. 7, no. 2, pp. 165–177, 1985.
- [8] A. Lopes, R. Touzi, and E. Nezry, "Adaptive speckle filters and scene heterogeneity," *IEEE Transactions on Geoscience and Remote Sensing*, vol. 28, pp. 992–1000, 1990.
- [9] M. Karaman, M. A. Kutay, and G. Bozdagi, "An adaptive speckle suppression filter for medical ultrasonic imaging," *IEEE Transactions on Medical Imaging*, vol. 14, no. 2, pp. 283–292, 1995. [Online]. Available: http://ieeexplore.ieee.org/xpls/abs_all.jsp?arnumber=387710
- [10] E. Kofidis, S. Theodoridis, C. Kotropoulos, and I. Pitas, "Nonlinear adaptive filters for speckle suppression in ultrasonic images," *Signal Processing*, vol. 52, no. 3, pp. 357–72, 1996. [Online]. Available: citeseer.ist.psu.edu/kofidis96nonlinear.html
- [11] J. M. Park, W. J. Song, and W. A. Pearlman, "Speckle filtering of sar images based on adaptive windowing," *Vision, Image and Signal Processing*, vol. 146, no. 4, pp. 191–197, 1999. [Online]. Available: http://ieeexplore.ieee.org/xpls/abs_all.jsp?arnumber=803320
- [12] P. C. Tay, S. T. Acton, and J. A. Hossack, "A stochastic approach to ultrasound despeckling," in *Biomedical Imaging: Nano to Macro, 2006. 3rd IEEE International Symposium on*, 2006, pp. 221–224. [Online]. Available: http://ieeexplore.ieee.org/xpls/abs_all.jsp?arnumber=1624892
- [13] —, "Ultrasound despeckling using an adaptive window stochastic approach," in *IEEE International Conference on Image Processing*, 2006, pp. 2549–2552. [Online]. Available: http://ieeexplore.ieee.org/xpls/abs_all.jsp?arnumber=4107088
- [14] T. C. Aysal and K. E. Barner, "Rayleigh-maximum-likelihood filtering for speckle reduction of ultrasound images," *IEEE Transactions on Medical Imaging*, vol. 26, no. 5, pp. 712–727, 2007. [Online]. Available: http://ieeexplore.ieee.org/xpls/abs_all.jsp?arnumber=4162627
- [15] P. Perona and J. Malik, "Scale-space and edge detection using anisotropic diffusion," *IEEE Transactions on Pattern Analysis and Machine Intelligence*, vol. 12, no. 7, pp. 629–639, 1990.
- [16] L. Rudin, S. Osher, and E. Fatemi, "Nonlinear total variation based noise removal algorithms," *Physica D*, vol. 60, pp. 259–268, 1992.
- [17] Y. Yu and S. T. Acton, "Speckle reducing anisotropic diffusion," *IEEE Transactions on Image Processing*, vol. 11, no. 11, pp. 1260–1270, 2002.
- [18] Y. Yu, J. A. Molloy, and S. T. Acton, "Three-dimensional speckle reducing anisotropic diffusion," in *Signals, Systems and Computers, 2003. Conference Record of the Thirty-Seventh Asilomar Conference on*, vol. 2, 2003, pp. 1987–1991 Vol.2. [Online]. Available: http://ieeexplore.ieee.org/xpls/abs_all.jsp?arnumber=1292329
- [19] K. Z. Abd-Elmoniem, A. B. Youssef, and Y. M. Kadam, "Real-time speckle reduction and coherence enhancement in ultrasound imaging via nonlinear anisotropic diffusion," *IEEE Transactions on Biomedical Engineering*, vol. 49, no. 9, pp. 997–1014, 2002. [Online]. Available: <http://www.ncbi.nlm.nih.gov/entrez/query.fcgi?cmd=Retrieve&db=pubmed&dopt=Abstract&listuids=12214889>
- [20] K. Krissian, C. F. Westin, R. Kikinis, and K. G. Vosburgh, "Oriented speckle reducing anisotropic diffusion," *IEEE Transactions on Image Processing*, vol. 16, no. 5, pp. 1412–1424, 2007. [Online]. Available: http://ieeexplore.ieee.org/xpls/abs_all.jsp?arnumber=4154795
- [21] C. Sheng, Y. Xin, Y. Liping, and S. Kun, "Total variation-based speckle reduction using multi-grid algorithm for ultrasound images," in *ICIAP: international conference on image analysis and processing*, vol. 3617, 2005, pp. 245–252.
- [22] K. Djemal, "Speckle reduction in ultrasound images by minimization of total variation," in *ICIP: international conference on image processing*, vol. 3, 2005, pp. 357–360.
- [23] D. Donoho and I. Johnstone, "Ideal spatial adaptation by wavelet shrinkage," *Biometrika*, vol. 81, no. 3, pp. 425–455, 1994.
- [24] D. Donoho, "De-noising by soft-thresholding," *IEEE Transactions on Information Theory*, vol. 41, no. 3, pp. 613–627, 1995.
- [25] R. Coifman and D. Donoho, "Translation invariant de-noising," in *Lecture Notes in Statistics: Wavelets and Statistics*, New York, February 1995, pp. 125–150.

- [26] J. E. Odegard, H. Guo, M. Lang, C. S. Burrus, R. O. Wells, L. M. Novak, and M. Hiett, "Wavelet based SAR speckle reduction and image compression," in *SPIE Proc. on Algorithms for Synthetic Aperture*, vol. 2487, 1995, pp. 259–271.
- [27] L. Gagnon and D. F. Smaili, "Speckle noise reduction of airborne sar images with symmetric daubechies wavelets," in *Proc. SPIE Signal and Data Processing of Small Targets*, O. E. Drummond, Ed., vol. 2759, 1996, pp. 14–24. [Online]. Available: <http://adsabs.harvard.edu/cgi-bin/nph-bib.query?bibcode=1996SPIE.2759...14G>
- [28] X. Zong, A. F. Laine, and E. A. Geiser, "Speckle reduction and contrast enhancement of echocardiograms via multiscale nonlinear processing," *IEEE Transactions on Medical Imaging*, vol. 17, no. 4, pp. 532–540, 1998. [Online]. Available: http://ieeexplore.ieee.org/xpls/abs_all.jsp?arnumber=730398
- [29] A. Pizurica, A. M. Wink, E. Vansteenkiste, W. Philips, and J. Roerdink, "A review of wavelet denoising in mri and ultrasound brain imaging," *Current Medical Imaging Reviews*, vol. 2, no. 2, pp. 247–260, 2006. [Online]. Available: <http://dx.doi.org/10.2174/157340506776930665>
- [30] A. Achim, A. Bezerianos, and P. Tsakalides, "Novel bayesian multiscale method for speckle removal in medical ultrasound images," *IEEE Transactions on Medical Imaging*, vol. 20, pp. 772–783, Aug. 2001. [Online]. Available: citeseer.comp.nus.edu.sg/484966.html
- [31] S. Foucher, G. B. Benie, and J. M. Boucher, "Multiscale map filtering of sar images," *IEEE Transactions on Image Processing*, vol. 10, no. 1, pp. 49–60, 2001. [Online]. Available: http://ieeexplore.ieee.org/xpls/abs_all.jsp?arnumber=892442
- [32] S. Gupta, R. C. Chauhan, and S. C. Saxena, "Locally adaptive wavelet domain bayesian processor for denoising medical ultrasound images using speckle modelling based on rayleigh distribution," *Vision, Image and Signal Processing, IEEE Proceedings*, vol. 152, no. 1, pp. 129–135, 2005. [Online]. Available: http://ieeexplore.ieee.org/xpls/abs_all.jsp?arnumber=1408933
- [33] M. I. H. Bhuiyan, Omair, and M. N. S. Swamy, "New spatially adaptive wavelet-based method for the despeckling of medical ultrasound images," in *IEEE International Symposium on Circuits and Systems, 2007. ISCAS 2007.*, 2007, pp. 2347–2350. [Online]. Available: http://ieeexplore.ieee.org/xpls/abs_all.jsp?arnumber=4253146
- [34] Z. Yang and M. D. Fox, "Speckle reduction and structure enhancement by multichannel median boosted anisotropic diffusion," *EURASIP J. Appl. Signal Process.*, vol. 2004, no. 1, pp. 2492–2502, January 2004. [Online]. Available: <http://portal.acm.org/citation.cfm?id=1289549>
- [35] O. Acosta, H. Frimmel, A. Fenster, and S. Ourselin, "Filtering and restoration of structures in 3d ultrasound images," in *Biomedical Imaging: From Nano to Macro, 2007. ISBI 2007. 4th IEEE International Symposium on*, 2007, pp. 888–891. [Online]. Available: http://ieeexplore.ieee.org/xpls/abs_all.jsp?arnumber=4193429
- [36] F. Zhang, Y. M. Yoo, L. M. Koh, and Y. Kim, "Nonlinear diffusion in laplacian pyramid domain for ultrasonic speckle reduction," *IEEE Transactions on Medical Imaging*, vol. 26, no. 2, pp. 200–211, 2007. [Online]. Available: http://ieeexplore.ieee.org/xpls/abs_all.jsp?arnumber=4077869
- [37] B. Aiazzi, L. Alparone, and S. Baronti, "Multiresolution local-statistics speckle filtering based on a ratio laplacian pyramid," *IEEE Transactions on Geoscience and Remote Sensing*, vol. 36, no. 5, pp. 1466–1476, 1998. [Online]. Available: http://ieeexplore.ieee.org/xpls/abs_all.jsp?arnumber=718850
- [38] X. Hao, S. Gao, and X. Gao, "A novel multiscale nonlinear thresholding method for ultrasonic speckle suppressing," *IEEE Transactions on Medical Imaging*, vol. 18, no. 9, pp. 787–794, 1999. [Online]. Available: <http://www.ncbi.nlm.nih.gov/entrez/query.fcgi?cmd=Retrieve&db=pubmed&dopt=Abstract&listuids=10571383>
- [39] A. Ogier, P. Hellier, and C. Barillot, "Restoration of 3D medical images with total variation scheme on wavelet domains (TVW)," in *SPIE Medical Imaging*, vol. 6144, February 2006.
- [40] M. Elad, "On the origin of the bilateral filter and ways to improve it," *IEEE Transactions on Image Processing*, vol. 11, no. 10, pp. 1141–1151, 2002.
- [41] C. Kervrann and J. Boulanger, "Optimal spatial adaptation for patch-based image denoising," *IEEE Transactions on Image Processing*, vol. 15, no. 10, 2006.
- [42] S. Kindermann, S. Osher, and P. W. Jones, "Deblurring and denoising of images by nonlocal functionals," *Multiscale Modeling & Simulation*, vol. 4, no. 4, pp. 1091–1115, 2005.
- [43] H. Q. Luong, A. Ledda, and W. Philips, "Non-local image interpolation," in *IEEE International Conference on Image Processing*, 2006, pp. 693–696. [Online]. Available: http://ieeexplore.ieee.org/xpls/abs_all.jsp?arnumber=4106624
- [44] T. Brox and D. Cremers, "Iterated nonlocal means for texture restoration," in *Proc. International Conference on Scale Space and Variational Methods in Computer Vision*, ser. LNCS. Ischia, Italy: Springer, May 2007.
- [45] C. Kervrann and J. Boulanger, "Local adaptivity to variable smoothness for exemplar-based image regularization and representation," *International Journal of Computer Vision*, 2008, accepted for future publication. [Online]. Available: <http://dx.doi.org/10.1007/s11263-007-0096-2>
- [46] P. Coupé, P. Yger, S. Prima, P. Hellier, C. Kervrann, and C. Barillot, "An Optimized Blockwise NonLocal Means Denoising Filter for 3-D Magnetic Resonance Images," *IEEE Transactions on Medical Imaging*, vol. 27, no. 4, pp. 425–441, April 2008.
- [47] Z. Tao, H. D. Tagare, and J. D. Beaty, "Evaluation of four probability distribution models for speckle in clinical cardiac ultrasound images," *IEEE Transactions on Medical Imaging*, vol. 25, no. 11, pp. 1483–1491, 2006. [Online]. Available: http://ieeexplore.ieee.org/xpls/abs_all.jsp?arnumber=1717646
- [48] G. Slabaugh, G. Unal, T. Fang, and M. Wels, "Ultrasound-specific segmentation via decorrelation and statistical region-based active contours," in *IEEE Computer Society Conference on Computer Vision and Pattern Recognition*, vol. 1, 2006, pp. 45–53.
- [49] K. Krissian, K. Vosburgh, R. Kikinis, and C.-F. Westin, "Speckle-constrained anisotropic diffusion for ultrasound images," in *IEEE Computer Society Conference on Computer Vision and Pattern Recognition*, June 2005.
- [50] F. Argenti and G. Torricelli, "Speckle suppression in ultrasonic images based on undecimated wavelets," *EURASIP Journal on Advances in Signal Processing*, vol. 2003, no. 5, pp. 470–478, 2003.
- [51] M. P. Wachowiak, A. S. Elmaghraby, R. Smolkova, and J. M. Zurada, "Classification and estimation of ultrasound speckle noise with neural networks," in *IEEE International Symposium on Bio-Informatics and Biomedical Engineering (BIBE'00)*, 2000, pp. 245–252.
- [52] D. Sakrison, "On the role of the observer and a distortion measure in image transmission," *IEEE Transactions on Communications*, vol. 25, no. 11, pp. 1251–1267, 1977. [Online]. Available: http://ieeexplore.ieee.org/xpls/abs_all.jsp?arnumber=1093773
- [53] J. A. Jensen, "Field: A program for simulating ultrasound systems," *Medical & Biological Engineering & Computing*, vol. 34, pp. 351–353, 1996.
- [54] P. Coupé, P. Hellier, X. Morandi, and C. Barillot, "Probe Trajectory Interpolation for 3D Reconstruction of Freehand Ultrasound," *Medical Image Analysis*, vol. 11, no. 6, pp. 604–615, 2007.
- [55] F. Godtliebsen, E. Spjøtvoll, and J. S. Marron, "A nonlinear gaussian filter applied to images with discontinuities," *J. Nonparametr. Statist.*, vol. 8, no. 1, pp. 21–43, 1997. [Online]. Available: <http://dx.doi.org/10.1080/10485259708832713>

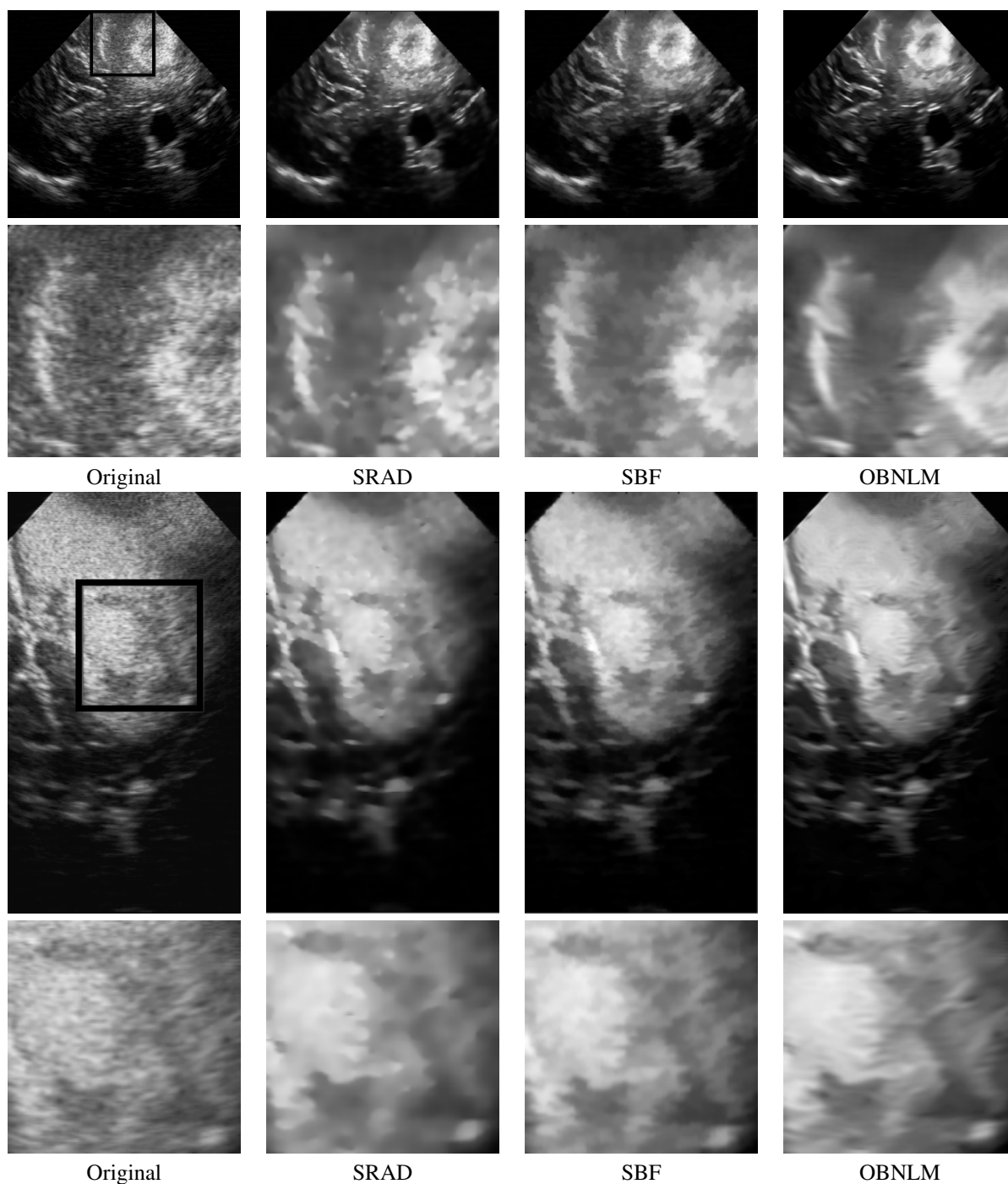


Fig. 5. Results obtained with the SRAD and SBF filters and the proposed filters on real intraoperative brain images. The OBNLM filter efficiently removes the speckle while enhancing the edges and preserving the image structures.

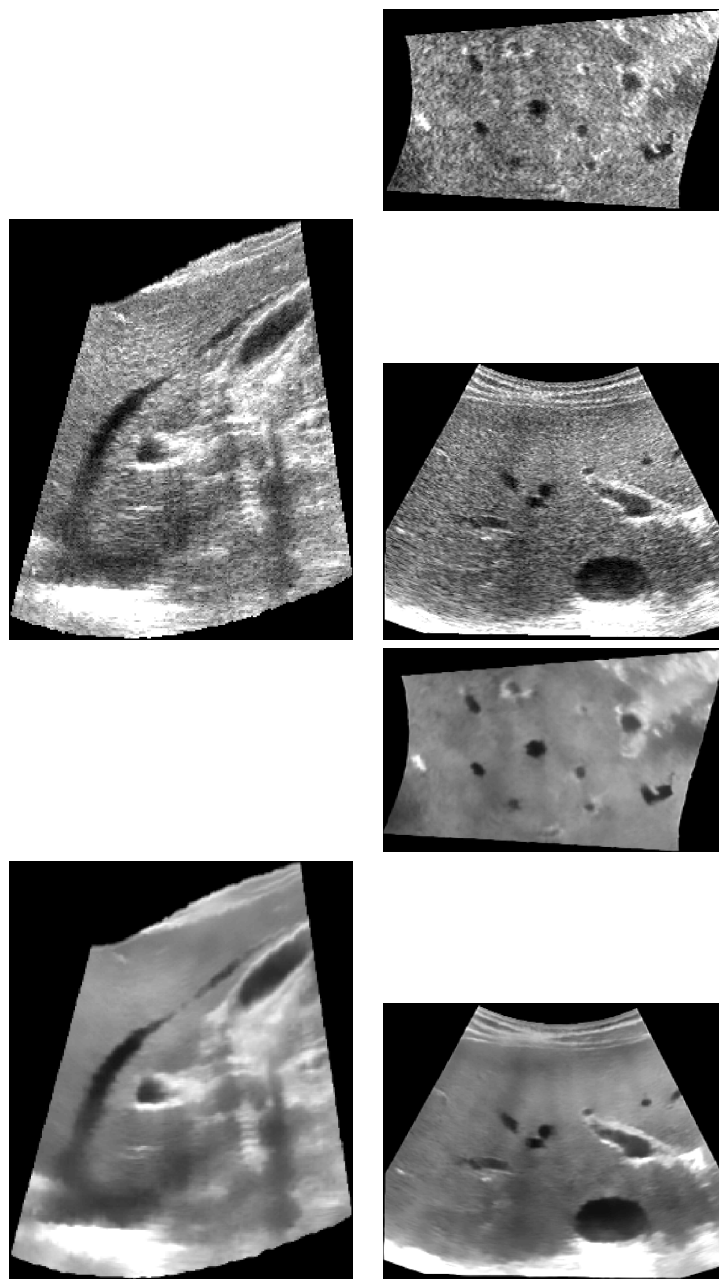


Fig. 6. Top: 3D volume of the liver. Bottom: the denoising result obtained with the OBNLM filter with $h = 8$, $n = 2$, $\alpha = 1$, $M = 5$ and $\mu_1 = 0.6$.

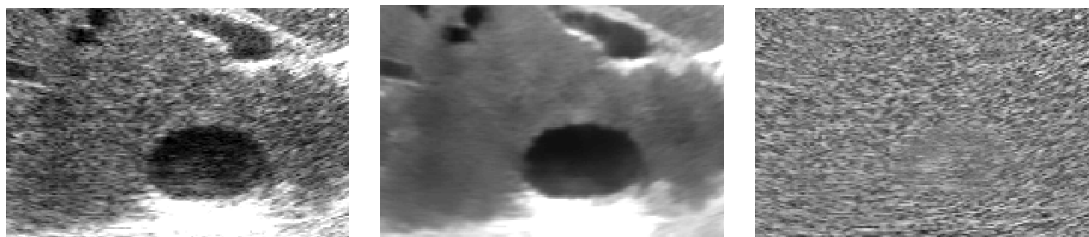


Fig. 7. From left to right: the original “noisy” volume, the denoising result obtained with the OBNLM filter with $h = 8$ and $\mu_1 = 0.6$ and the removed noise component. The edge preservation of the OBNLM is visually appreciated by inspecting the removed noise component which contains few structures. Moreover, the level of noise estimated for the dark areas (hepatic vessels) and the gray areas (hepatic tissues) demonstrates the relevance of the signal-dependent modeling.